


Sound propagation in porous materials containing rough tubes

Cite as: Phys. Fluids **32**, 093604 (2020); <https://doi.org/10.1063/5.0017710>

Submitted: 10 June 2020 . Accepted: 12 August 2020 . Published Online: 03 September 2020

Zhimin Xu, Wei He, Fengxian Xin , and Tian Jian Lu

COLLECTIONS

 This paper was selected as an Editor's Pick



View Online



Export Citation



CrossMark

ARTICLES YOU MAY BE INTERESTED IN

[Visualizing droplet dispersal for face shields and masks with exhalation valves](#)

Physics of Fluids **32**, 091701 (2020); <https://doi.org/10.1063/5.0022968>

[Azimuthal instability of the radial thermocapillary flow around a hot bead trapped at the water-air interface](#)

Physics of Fluids **32**, 092108 (2020); <https://doi.org/10.1063/5.0018711>

[Ultrafast tomographic particle image velocimetry investigation on hypersonic boundary layers](#)

Physics of Fluids **32**, 094103 (2020); <https://doi.org/10.1063/5.0014168>



NEW!

Sign up for topic alerts
New articles delivered to your inbox



Sound propagation in porous materials containing rough tubes

Cite as: Phys. Fluids 32, 093604 (2020); doi: 10.1063/5.0017710

Submitted: 10 June 2020 • Accepted: 12 August 2020 •

Published Online: 3 September 2020



View Online



Export Citation



CrossMark

Zhimin Xu,^{1,2} Wei He,^{1,2} Fengxian Xin,^{1,2,a)}  and Tian Jian Lu^{3,4,b)}

AFFILIATIONS

¹State Key Laboratory for Strength and Vibration of Mechanical Structures, Xi'an Jiaotong University, Xi'an 710049, People's Republic of China

²MOE Key Laboratory for Multifunctional Materials and Structures, Xi'an Jiaotong University, Xi'an 710049, People's Republic of China

³State Key Laboratory of Mechanics and Control of Mechanical Structures, Nanjing University of Aeronautics and Astronautics, Nanjing 210016, People's Republic of China

⁴Nanjing Center for Multifunctional Lightweight Materials and Structures (MLMS), Nanjing University of Aeronautics and Astronautics, Nanjing 210016, People's Republic of China

^{a)}Author to whom correspondence should be addressed: fengxian.xin@gmail.com

^{b)}tjlu@nuaa.edu.cn

ABSTRACT

A theoretical model is developed to quantify the influence of surface roughness on sound propagation in porous materials containing rough tubes by extending the Johnson–Champoux–Allard–Lafarge (JCAL) model. The five transport parameters of the JCAL model, including the viscous permeability, thermal permeability, tortuosity, viscous characteristic length, and thermal characteristic length, are calculated by modeling the rough tubes in the porous material as parallel rough tubes having idealized sinusoidal morphologies. The transport parameters obtained using the proposed model are validated by full finite element simulations. Based on these transport parameters, the sound absorption coefficient of the porous material containing idealized rough tubes is calculated, which agrees well with the FE result. The roughness effect is investigated by comparing sound absorption performance between parallel smooth tubes and parallel rough tubes. The existence of tube roughness weakens the thermal effect but dramatically strengthens the viscous effect in sound energy dissipation, resulting in enhanced sound absorption. This work provides fundamental insights on how surface roughness affects the acoustic performance of sound-absorbing porous materials.

Published under license by AIP Publishing. <https://doi.org/10.1063/5.0017710>

I. INTRODUCTION

Sound propagation in a porous medium is a typical fluid mechanics problem relating to physical properties of the fluid and thermal properties of the medium as sound energy is dissipated mainly via viscous and heat losses. To address these properties, a simple way is to regard the porous medium as a series of uniformly distributed cylindrical tubes parallel to each other, enabling the determination of these properties theoretically. Based on this simplified model, Kirchhoff¹ and Rayleigh² presented exact solutions for sound propagation in uniform circular tubes by taking the effects of both air viscosity and thermal conductivity into consideration. Although Kirchhoff's theory is fully theoretical and

characterizes the sound absorbing performance of cylindrical tubes precisely, the intrinsic physical equations are unnecessarily complicated for many practical applications. More applicable solutions^{3–6} were latterly proposed by separately treating the viscous effect and the thermal effect, with the complex density and compressibility functions found to be responsible for these two effects. To extend the models for circular tubes to non-circular tubes, the concept of shape factor was introduced to quantify the influence of tubes having arbitrary cross sections.^{7,8} Upon introducing the concept of tortuosity, static flow resistivity, and porosity, sound propagation in porous materials can be characterized using the parallel circular tube model, which is actually a simple but valid way to avoid the randomness of typical porous materials.⁹

Theoretical models are powerful for understanding the physical mechanisms underlying sound propagation in a series of parallel smooth tubes. However, the widely applied smooth tube assumption is not sufficiently accurate to evaluate the sound absorbing performance of many porous materials. The surface roughness of the tubes significantly affects fluid flow in a porous material and hence cannot be ignored when considering sound propagation. How surface roughness influences the in-tube fluid flow has been investigated for years. For example, Colebrook *et al.*^{10–12} and Nikuradse *et al.*^{10–12} conducted detailed experimental and theoretical research studies on the influence of uniform surface roughness and Reynolds number on fluid flow in rough pipes. They demonstrated that the effect of surface roughness can be divided into different regions and proposed several empirical formulas to quantify the roughness effect. Based on these experimental and theoretical works, Moody¹³ plotted a diagram (i.e., the Moody chart) of the relationship among relative roughness, Reynolds number, and Darcy friction factor, useful in industrial applications. However, these studies only considered relatively low relative roughness (i.e., <5%), which means that the conclusions cannot be directly applied when the relative roughness exceeds 5%. For cases of high relative roughness or high Reynolds number, a series of theoretical and numerical research studies were carried out to calculate the fluid field in a rough pipe by assuming a periodic structure upon the boundary of the pipe.^{14–23} These studies led to an important conclusion that the existence of wall roughness on laminar and incompressible flow in pipes increases the pressure drop and static flow resistivity. More recently, upon modeling the surface roughness as a sinusoidal type, we investigated fully developed steady laminar flow in circular pipes and obtained analytical solution of flow field using the perturbation theory by regarding the surface roughness as a disturbance on the pipe boundary.²⁴

Although fluid flow inside a rough pipe has been studied both theoretically and experimentally, few works exist on sound propagation in porous materials containing rough tubes. A feasible way to characterize the sound absorption performance of a porous material is describing its equivalent fluid properties by all means, which requires determining relevant viscous and thermal parameters of the material. Based on this approach, Ren *et al.*²⁵ proposed a semi-analytical model for sound propagation in sintered metal fiber materials and quantified the influence of temperature on sound absorption. For a porous material with idealized rough pores, Yang *et al.*²⁶ presented an analytical model to predict its permeability by constructing a three-dimensional (3D) cubic unit cell that has cylindrical micro-rods synthesized on cell walls. Liu *et al.*²⁷ experimentally demonstrated that the copper fiber sintered sheets with a rough surface exhibited better sound absorption performance compared with those with a smooth surface. However, to clearly describe the influence of roughened surface on sound propagation in porous materials, a full investigation needs to be performed. To this end, in the current study, we develop a theoretical model to quantify the influence of surface roughness on sound propagation by describing the porous material with the Johnson–Champoux–Allard–Lafarge (JCAL) model. The JCAL model is a widely used equivalent fluid model suitable for all kinds of porous materials. With the roughened pore surfaces idealized as the sinusoidal type, the viscous and thermal parameters of the porous material are derived analytically, thus enabling to calculate its equivalent density and equivalent

modulus and hence its sound absorption coefficient. Other types of surface roughness, for example, triangular, rectangular, and random morphologies,²⁷ can also be studied by expanding the morphology function into a series of sinusoidal functions.²⁴ For validation, a full 3D finite element (FE) model is established. The results obtained in the present paper are helpful for tailoring the pore morphologies of porous materials to achieve superior acoustic property. Though the theoretical model in this paper is based on idealized sinusoidal pore morphologies of porous materials, the results of this paper can provide fundamental insights on how surface roughness affects the acoustic performance of sound-absorbing porous materials.

II. THEORETICAL MODEL

When sound propagates in a porous material sample, its sound absorption performance is strongly affected by surface roughness of the pores, for its static flow resistivity and tortuosity depend on surface roughness. Theoretically, sound absorption can be characterized by incorporating the semi-phenomenological model of Johnson–Champoux–Allard–Lafarge (JCAL) and the dependence of equivalent fluid parameters of the porous material upon surface roughness. The JCAL model²⁸ describes sound propagation in the porous material based on two equivalent fluid properties, the equivalent density $\rho_{eq}(\omega)$ and the equivalent bulk modulus $K_{eq}(\omega)$,

$$\begin{aligned} \rho_{eq}(\omega) &= \frac{\alpha_\infty \rho_0}{\phi} \left[1 + \frac{\mu \phi}{j \omega \rho_0 \alpha_\infty} \sqrt{1 + j \frac{4 \alpha_\infty^2 \hat{k}_0^2 \omega \rho_0}{\mu \phi^2 \Lambda^2}} \right], \\ K_{eq}(\omega) &= \frac{\gamma P_0}{\phi} \left/ \left\{ \gamma - (\gamma - 1) \left/ \left[1 - j \frac{\phi \kappa}{\hat{k}'_0 C_p \rho_0 \omega} \right. \right. \right. \right. \\ &\quad \left. \left. \left. \times \sqrt{1 + j \frac{4 \hat{k}_0^2 C_p \rho_0 \omega}{\kappa \Lambda^2 \phi^2}} \right] \right\} \right., \end{aligned} \quad (1)$$

where the static density is $\rho_0 = 1.23 \text{ kg m}^{-3}$, the dynamic viscosity is $\mu = 1.84 \times 10^{-5} \text{ Pa s}$, the specific heat capacity at constant pressure is $C_p = 1006 \text{ J kg}^{-1} \text{ K}^{-1}$, the specific heat ratio is $\gamma = 1.4$, and the heat conductivity of air is $\kappa = 0.025 \text{ W m}^{-1} \text{ K}^{-1}$, which are all independent of surface roughness; ϕ is the porosity, $j = \sqrt{-1}$ is the imaginary unit, and ω is the angular frequency of sound waves. In contrast, the transport parameters (i.e., viscous permeability \hat{k}_0 , thermal permeability \hat{k}'_0 , tortuosity α_∞ , viscous characteristic length Λ , and thermal characteristic length Λ') are all closely related to surface roughness. As described in Eq. (1), the viscous and thermal interactions between the air and the solid skeleton of the porous material affect the equivalent fluid properties, which makes the static density ρ_0 and modulus γP_0 of air convert into the frequency-dependent equivalent fluid properties $\rho_{eq}(\omega)$ and $K_{eq}(\omega)$. Once these equivalent fluid properties are determined, the sound absorption performance of the porous material can be deduced by analyzing its characteristic impedance and propagation constant.

To address the equivalent fluid properties $\rho_{eq}(\omega)$ and $K_{eq}(\omega)$, the transport parameters, \hat{k}_0 , \hat{k}'_0 , α_∞ , Λ , and Λ' , need to be determined first. With reference to Fig. 1, the parallel rough tube model is adopted to calculate the transport parameters of the porous material having idealized sinusoidal pores. Let D be the mean diameter of

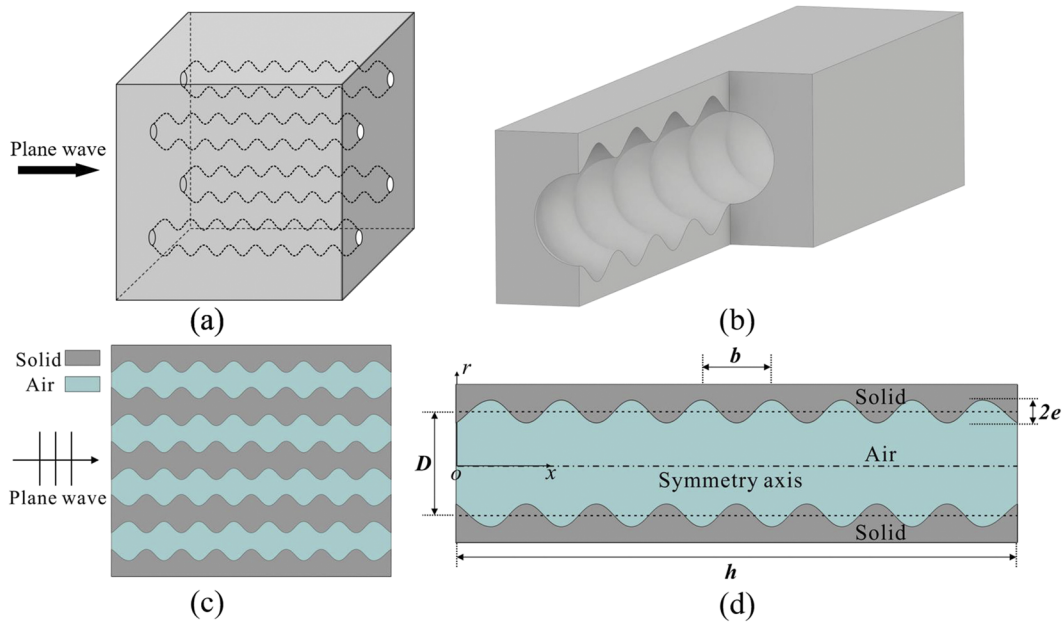


FIG. 1. Schematic of the parallel rough tube model for the porous material: (a) parallel rough tube model, (b) one unit cell, (c) half section cut view, and (d) two-dimensional view of one rough tube.

the rough tube, and let e and b be the amplitude and wavelength of the sinusoidal roughness. The radius of the rough tube (i.e., r) varies with the position (i.e., x) changes, and it can be expressed as

$$r(x) = D \left[\frac{1}{2} - \varepsilon \cos(\beta \tilde{x}) \right], \quad (2)$$

where $\varepsilon = e/D$ is the relative roughness to quantify the amplitude of the roughness, $\beta = 2\pi D/b$ is the wave number to describe the intensity of the roughness, and $\tilde{x} = x/D$ is the dimensionless position. According to the definition of viscous dynamic permeability,²⁹ the viscous permeability \hat{k}_0 is actually the limit of viscous dynamic permeability when ω tends to zero. So, the surface dependent viscous permeability can be described as

$$\hat{k}_0 = \lim_{\omega \rightarrow 0} \frac{\mu \phi}{j \omega \rho_{\text{eq}}(\omega)}. \quad (3)$$

From the definition of flow resistivity, the viscous permeability \hat{k}_0 can be expressed as a function of the flow resistivity of the porous material σ_m ,

$$\hat{k}_0 = \frac{\mu}{\sigma_m}. \quad (4)$$

Because the parallel tubes are distributed uniformly, σ_m can be determined from the flow resistivity of a single rough tube σ_t as $\sigma_m = \sigma_t/\phi$. Regarding the sinusoidal roughness as a disturbance of the tube boundary, Song *et al.*²⁴ calculated the flow resistivity of a rough tube using the perturbation theory as

$$\sigma_t = \frac{32\mu}{D^2} \left\{ \left(\frac{6\varepsilon^2 + 1}{(1 - 4\varepsilon^2)^{3.5}} - \frac{1}{(1 - 2\varepsilon)^4} \right) \frac{2e^{-\frac{1}{5\pi}\beta}}{1 + e^{-\frac{1}{5\pi}\beta}} + \frac{1}{(1 - 2\varepsilon)^4} \right\}, \quad (5)$$

where $32\mu/D^2$ denotes the flow resistivity of a smooth circular tube of diameter D . From Eq. (5), one can find that the flow resistivity of a rough tube is significantly greater than its smooth counterpart. Similarly, upon using the perturbation method, the tortuosity of the rough tube α_∞ can be determined by³⁰

$$\alpha_\infty = 1 + \frac{\varepsilon^2 \beta^2 [(J_0^2(\beta/2) - J_1^2(\beta/2))]}{2J_1^2(\beta/2)}, \quad (6)$$

where $J_0(\cdot)$ is the modified Bessel function of the first kind and zeroth order and $J_1(\cdot)$ is the modified Bessel function of the first kind and first order.

The viscous characteristic length of a porous material Λ , which actually describes the hydraulic radius of the porous material, is derived in the limit of high frequencies where the viscous boundary layer becomes extremely thin, and the fluid in the porous material can be regarded as an ideal inviscid fluid as

$$\frac{2}{\Lambda} = \frac{\int_A v_i^2(\mathbf{r}_w) dA}{\int_V v_i^2(\mathbf{r}) dV}. \quad (7)$$

For a static flow of inviscid fluid in the porous medium, $v_i(\mathbf{r}_w)$ is the fluid velocity at the position coordinates \mathbf{r}_w on the pore surface, and the integration in the numerator is over surface A of the pore in the representative elementary volume. $v_i(\mathbf{r})$ is the velocity of fluid at the position coordinates \mathbf{r} inside the pores, and the integration in the denominator is over the volume V of the pore. Here, the viscous characteristic length, representing the hydraulic radius of the porous material, can be calculated using its relationship with flow resistivity as³¹

$$\Lambda = \left(\frac{8\mu\alpha_\infty}{\sigma_m\phi} \right)^{1/2}. \quad (8)$$

Similarity, the thermal characteristic length of the porous material Λ' , which greatly influences the equivalent bulk modulus of the porous medium, as shown in Eq. (1), is given by

$$\frac{2}{\Lambda'} = \frac{\int_A dA}{\int_V dV}. \quad (9)$$

The integral in the numerator is performed over the pore surface A in the representative elementary volume, and the denominator is performed over the volume V of the pore, with respect to Eq. (7); there is no weighting by the squared velocity. For the case of a rough tube in the sinusoidal shape, as shown in Fig. 1, the integral over the pore surface A can be expressed as

$$\int_A dA = \int 2\pi r(x)\sqrt{1+r'^2(x)}dx, \quad (10)$$

while the integral over the pore volume V can be expressed as

$$\int_V dV = \int \pi r^2(x)dx, \quad (11)$$

where the position related radius is described by Eq. (2).

The thermal permeability \hat{k}'_0 has been defined by Lafarge *et al.*³² It is a complex parameter relating the pressure time derivative to mean temperature. Champoux and Allard³³ proposed a simple yet accurate expression that relates thermal permeability to porosity ϕ and thermal characteristic length Λ' as

$$\hat{k}'_0 = \frac{\phi\Lambda'^2}{8}. \quad (12)$$

This expression is adopted in the current study.

Hitherto, the five transport parameters, \hat{k}_0 , \hat{k}'_0 , α_∞ , Λ , and Λ' , are all determined directly using structural (morphological) parameters of the porous material, i.e., porosity ϕ , relative roughness ϵ , and wave number β . The equivalent density $\rho_{eq}(\omega)$ and the equivalent bulk modulus $K_{eq}(\omega)$ of the porous material can be calculated by substituting the five transport parameters into the JCAL model, i.e., Eq. (1). To analyze the sound absorbing performance, the characteristic impedance $Z_m(\omega)$ and the propagation constant $k_m(\omega)$ of the porous material are determined by

$$\begin{aligned} Z_m(\omega) &= \sqrt{\rho_{eq}(\omega)K_{eq}(\omega)}, \\ k_m(\omega) &= j\omega\sqrt{\rho_{eq}(\omega)/K_{eq}(\omega)}. \end{aligned} \quad (13)$$

For a rigid-backed porous material (with thickness h), the surface impedance is given by

$$Z_s(\omega) = Z_m(\omega) \coth(k_m(\omega) \cdot h). \quad (14)$$

Finally, the sound absorption coefficient of the porous material containing rough tubes can be expressed as

$$\alpha = 1 - \left| \frac{Z_s - Z_0}{Z_s + Z_0} \right|^2, \quad (15)$$

where $Z_0 = \rho_0 c_0$ is the characteristic impedance of air.

III. NUMERICAL MODEL

The full 3D finite element model is developed to validate the above theoretical model. To this end, the multi-scale asymptotic method^{31,34} is applied to calculate the transport parameters of the porous material. In the model, three sets of equations, namely, the viscous flow equations, the inertial flow equations, and the thermal conduction equations, need to be solved independently.

When the frequency of the sound wave is close to 0, the motion of fluid is dominated by the viscosity of the fluid. Under the external excitation of a pressure gradient \mathbf{g} , the microscopic velocity \mathbf{v}_m and the sound pressure p_m in the fluid domain Ω_f must satisfy the static Stokes equation as

$$\mu\Delta\mathbf{v}_m = \nabla p_m + \mathbf{g} \text{ in } \Omega_f, \quad (16)$$

$$\nabla \cdot \mathbf{v}_m = 0 \text{ in } \Omega_f. \quad (17)$$

At the solid–fluid interfaces $\partial\Omega_{sf}$, no-slip boundary conditions are adopted as

$$\mathbf{v}_m = \mathbf{0} \text{ on } \partial\Omega_{sf}. \quad (18)$$

According to Darcy's law, the microscopic velocity \mathbf{v}_m is related to the viscous permeability vector \mathbf{k}_0 as $\mathbf{v}_m = -|\mathbf{g}|\mathbf{k}_0/\mu$. In addition, a scalar pressure field is defined as $q_0 = -p_m/|\mathbf{g}|$. Then, the static Stokes equation and the no-slip free boundary conditions are transformed into the following forms:

$$\Delta\mathbf{k}_0 = \nabla q_0 - \mathbf{e} \text{ in } \Omega_f, \quad (19)$$

$$\nabla \cdot \mathbf{k}_0 = 0 \text{ in } \Omega_f, \quad (20)$$

$$\mathbf{k}_0 = \mathbf{0} \text{ on } \partial\Omega_{sf}, \quad (21)$$

where \mathbf{e} is a unit vector along the direction of pressure gradient \mathbf{g} .

The viscosity permeability \hat{k}_0 can be calculated as

$$\hat{k}_0 = \phi \langle k_0^m \rangle, \quad (22)$$

where k_0^m is the component of \mathbf{k}_0 along the propagation direction of sound wave and the operator $\langle \rangle$ indicates a volume average over the fluid domain.

As the frequency of the sound wave approaches infinity, the viscosity of fluid becomes negligible. When the fluid passes through the porous material, its motion is dominated by inertial effects. In this case, the fluid flow problem is equivalent to the problem of electrical conductivity of a conductive fluid within the insulating skeleton of a porous material,^{35–37} as:

$$\mathbf{E} = \mathbf{e}' - \nabla q \text{ in } \Omega_f, \quad (23)$$

$$\nabla \cdot \mathbf{E} = 0 \text{ in } \Omega_f, \quad (24)$$

where the unit vector \mathbf{e}' is the externally applied macroscopic electric field, \mathbf{E} is the local electric field, $-\nabla q$ is the disturbance term of \mathbf{E} , and \mathbf{n} is the normal vector on the fluid–solid interface. The walls of the skeleton satisfy the insulation boundary condition as

$$\mathbf{E} \cdot \mathbf{n} = 0 \text{ on } \partial\Omega_{sf}. \quad (25)$$

Once the local electric field is determined, the tortuosity α_∞ , the viscous characteristic length Λ , and the thermal characteristic length Λ' can be obtained as follows:

$$\alpha_\infty = \frac{\langle \mathbf{E} \cdot \mathbf{E} \rangle}{\langle \mathbf{E} \rangle \cdot \langle \mathbf{E} \rangle}, \quad (26)$$

$$\Lambda = 2 \frac{\int_{\Omega_f} \mathbf{E} \cdot \mathbf{E} dV}{\int_{\partial\Omega_{sf}} \mathbf{E} \cdot \mathbf{E} dS}, \quad (27)$$

$$\Lambda' = 2 \frac{\int_{\Omega_f} dV}{\int_{\partial\Omega_{sf}} dS}. \quad (28)$$

When the sound wave propagates in a fluid, the fluctuation of sound pressure causes compression/expansion of the fluid, resulting in fluctuation of fluid temperature T . The temperature field in the fluid domain is controlled by the heat conduction equation. Because the thermal conductivity of the fluid (such as air) is generally far less than that of the solid skeleton of porous materials, the isothermal boundary condition is adopted at fluid–solid interfaces. The governing equations together with the boundary condition are

$$\kappa \Delta T - i\omega C_p \rho_0 T = -i\omega P \text{ in } \Omega_f, \quad (29)$$

$$T = 0 \text{ on } \partial\Omega_{sf}, \quad (30)$$

where κ is the thermal conductivity of the fluid, C_p is the specific heat at constant pressure, and P is the fluid pressure. With the thermal dynamic permeability denoted by k' , the temperature can be linked to the pressure P as $T = i\omega P k' / \kappa$.³² At low frequencies, the governing equation and the boundary condition can be simplified into

$$-\Delta k'_0 = 1 \text{ in } \Omega_f, \quad (31)$$

$$k'_0 = 0 \text{ on } \partial\Omega_{sf}. \quad (32)$$

The thermal permeability \hat{k}'_0 is determined by

$$\hat{k}'_0 = \phi \langle k'_0 \rangle. \quad (33)$$

IV. RESULTS AND DISCUSSION

To validate the proposed theoretical model, full numerical simulations are carried out to evaluate the sound absorption performance of parallel rough and smooth tubes, separately representing porous materials with and without the roughness effect in the pores. Relevant structure parameters are adopted as $D = 0.6$ mm, $\varepsilon = 0.2$, $\beta = 1$, $\phi = 34.91\%$, and $h = 30$ mm. For the choice of these parameters, it was reported that the optimal cell size of porous materials for best sound absorption was on the order of ~ 0.1 mm.³⁸ Therefore, the mean diameter of the rough tube $D = 0.6$ mm represents a moderate size. The relative roughness ε is no more than 0.2, which ensures the accuracy of theoretical predictions for transport parameters.²⁴ The value of the wavenumber β , the porosity ϕ , and the thickness h has no specific limit. The choice of $\beta = 1$, $\phi = 34.91\%$, and $h = 30$ mm is just to obtain good low-frequency sound absorption performance without wasting too much material. The porosity of 34.91% corresponds to the situation in which the horizontal

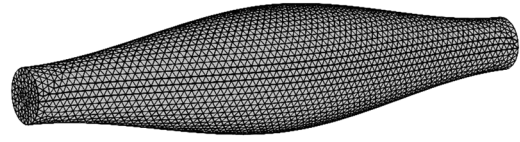


FIG. 2. Finite element model for a periodic segment of the rough tube.

and vertical spacing of rough tubes are all 0.9 mm. For the porous material containing rough tubes, a periodic segment of the rough tube is selected as the computational model, and the FE mesh is shown in Fig. 2.

Three modules of the commercial FE code COMSOL Multiphysics, namely, the Creep Flow module, the Electrostatics module, and the Coefficient Form partial differential equations (PDE) module, are used to solve three sets of partial differential equations of the numerical model. In the Creep Flow module, the density and dynamic viscosity of the fluid are set to 1 kg/m^3 and 1 Pa s , respectively, and the governing equation of the fluid is transformed into the form of Eq. (19). The value of pressure at the inlet is equal to that of the unit cell length, while the pressure at the outlet is set to 0 Pa, which is equivalent to externally applying a macroscopic unit pressure gradient. Similarly, to apply a macroscopic unit electric field in the Electrostatics module, the value of electric potential at the inlet is equal to that of the unit cell length, while the electric potential at the outlet is set to 0 V. The coefficients of the built-in differential equation in the Coefficient Form PDE module can be determined according to the form of Eq. (31). At the fluid–solid interface, the Dirichlet boundary condition is applied.

To ensure the accuracy of the numerical calculations, a mesh convergence study is implemented, as listed in Table I. In the FE simulations, as the number of elements increases, the numerical results tend to the corresponding convergence solutions. However, the finer the mesh, the more computing resources it takes up. Therefore, the penultimate set of the mesh element number in Table I is adopted for numerical calculations, and the convergence results are used for sound absorption calculations.

In Table II, the five transport parameters of the considered porous material (Fig. 1) obtained using the present theoretical model are compared with those calculated numerically. The theoretically predicted transport parameters are calculated with the corresponding equations, i.e., Eq. (4) for viscous permeability, Eq. (12) for thermal permeability, Eq. (6) for tortuosity, Eq. (8) for viscous characteristic length, and Eq. (9) for thermal characteristic length. For the case considered here, a good agreement is achieved between theoretical model predictions and FE simulation results. Among all the five transport parameters, only the thermal permeability has a relatively large error between the theoretical prediction and the numerical result. However, the influence of thermal permeability on sound absorption is much less than that of viscous permeability. Consequently, the present theoretical predictions are accurate enough for predicting sound absorption in porous materials containing rough tubes.

Substituting the five transport parameters into the JCAL model and calculating the sound absorption coefficient via Eq. (15) enable theoretically determining the sound absorption coefficient for both parallel rough tubes and smooth tubes. With reference to Fig. 3,

TABLE I. A mesh convergence study for the numerically calculated transport parameters.

Number of elements	$\hat{k}_0/(10^{-3} \text{ mm}^2)$	α_∞	Λ (mm)	Λ' (mm)	$\hat{k}'_0/(10^{-3} \text{ mm}^2)$
154 287	1.5956	1.4048	0.231 95	0.319 49	5.1994
456 185	1.6055	1.4033	0.232 51	0.319 86	5.2055
728 048	1.6084	1.4029	0.232 68	0.319 95	5.2070
981 806	1.6098	1.4026	0.232 77	0.320 00	5.2077
1 268 579	1.6108	1.4025	0.232 83	0.320 03	5.2083
1 528 371	1.6112	1.4023	0.232 87	0.320 05	5.2086
1 630 639	1.6112	1.4023	0.232 87	0.320 06	5.2087
1 742 814	1.6112	1.4023	0.232 87	0.320 06	5.2087

TABLE II. Theoretical predictions and numerical results of transport parameters.

Acoustic parameters	Symbol	Theoretical predictions R_t	Numerical results R_n	Relative error $\delta = R_t - R_n /R_n$ (%)
Viscous permeability	$\hat{k}_0/(10^{-3} \text{ mm}^2)$	1.5994	1.611 2	0.73
Thermal permeability	$\hat{k}'_0/(10^{-3} \text{ mm}^2)$	4.6946	5.208 7	9.87
Tortuosity	α_∞	1.3201	1.402 3	5.86
Viscous characteristic length	Λ (mm)	0.21196	0.232 87	8.98
Thermal characteristic length	Λ' (mm)	0.32799	0.320 06	2.48

the solid line represents theoretical predictions, while the symbols indicate FE simulation results. As shown in Fig. 3, for both parallel rough tubes and smooth tubes, the predicted absorption coefficients show good agreements with the numerical results. Compared to the smooth tubes, the rough tubes exhibit a better sound absorption performance, which means a lower peak frequency and a higher

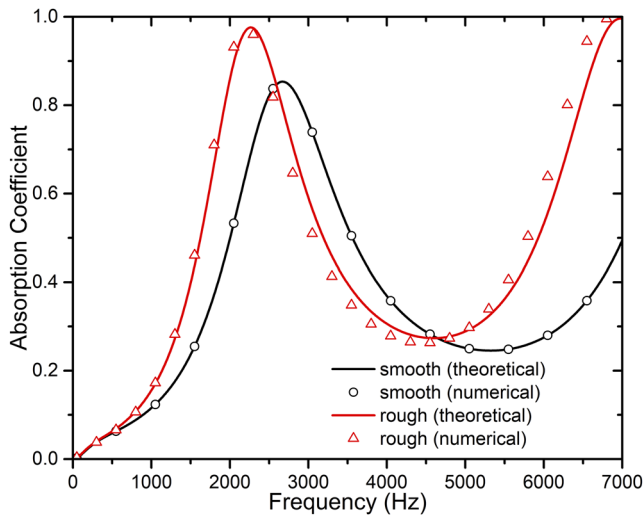


FIG. 3. The theoretical and numerical results of the sound absorption coefficient for parallel rough tubes and smooth tubes.

absorption peak value. More specifically, the first absorption coefficient peak of the parallel rough tubes is about 0.97 at 2290 Hz, while that of the parallel smooth tubes is about 0.85 at 2670 Hz. The absorption peak increases by 14.1%, while the peak frequency decreases by 14.2%.

To reveal the reason why the sound absorption performance of the rough tubes deviates from the smooth ones, sound energy dissipation (which consists of thermal and viscous effects) needs to be analyzed. Both the thermal and viscous effects are strongly related to the five transport parameters. The transport parameters $\hat{k}_0 = \hat{k}'_0 = 3.9274 \times 10^{-3} \text{ mm}^2$, $\alpha_\infty = 1$, $\Lambda = \Lambda' = 0.3 \text{ mm}$ obtained for parallel smooth tubes are all far different from those listed in Table I for parallel rough tubes. Specifically, the thermal permeability and thermal characteristic length of rough tubes are both

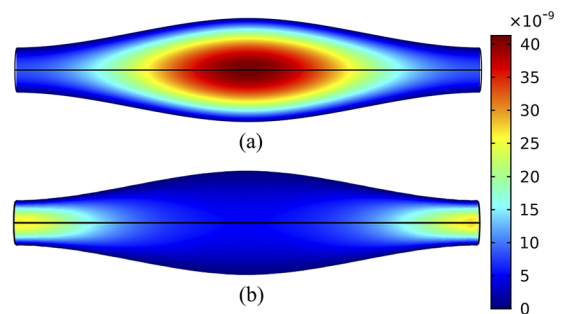


FIG. 4. Numerical results for a periodic segment of the rough tube: (a) thermal permeability distribution (m^2) and (b) viscous permeability distribution (m^2).

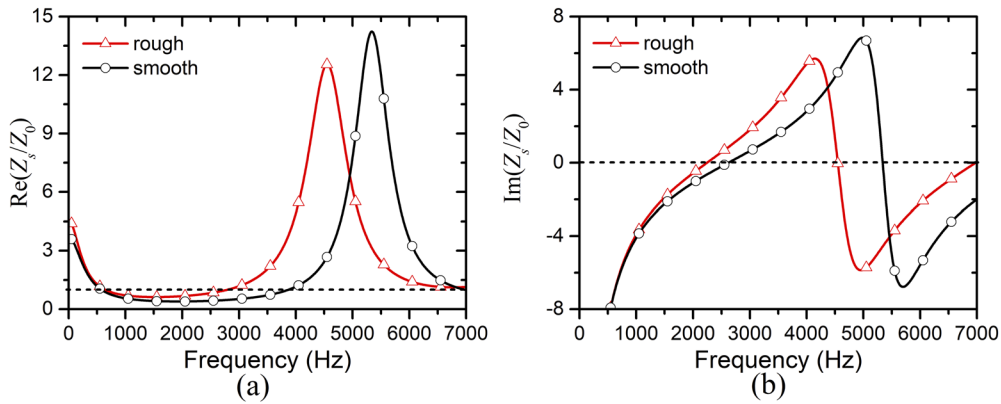


FIG. 5. (a) The real part and (b) imaginary part of normalized surface impedance of parallel rough tubes and parallel smooth tubes.

larger than those of smooth tubes, which indicates a smaller thermal effect when energy dissipates from the rough tubes. However, both the viscous permeability and viscous characteristic length are smaller than those of smooth tubes, indicating a larger viscous effect

when sound propagates in rough tubes. In fact, when a sound wave travels in parallel tubes, the existence of surface roughness makes the air inside the tubes more difficult to be compressed, resulting in a smaller temperature rise of the air. The thermal effect is

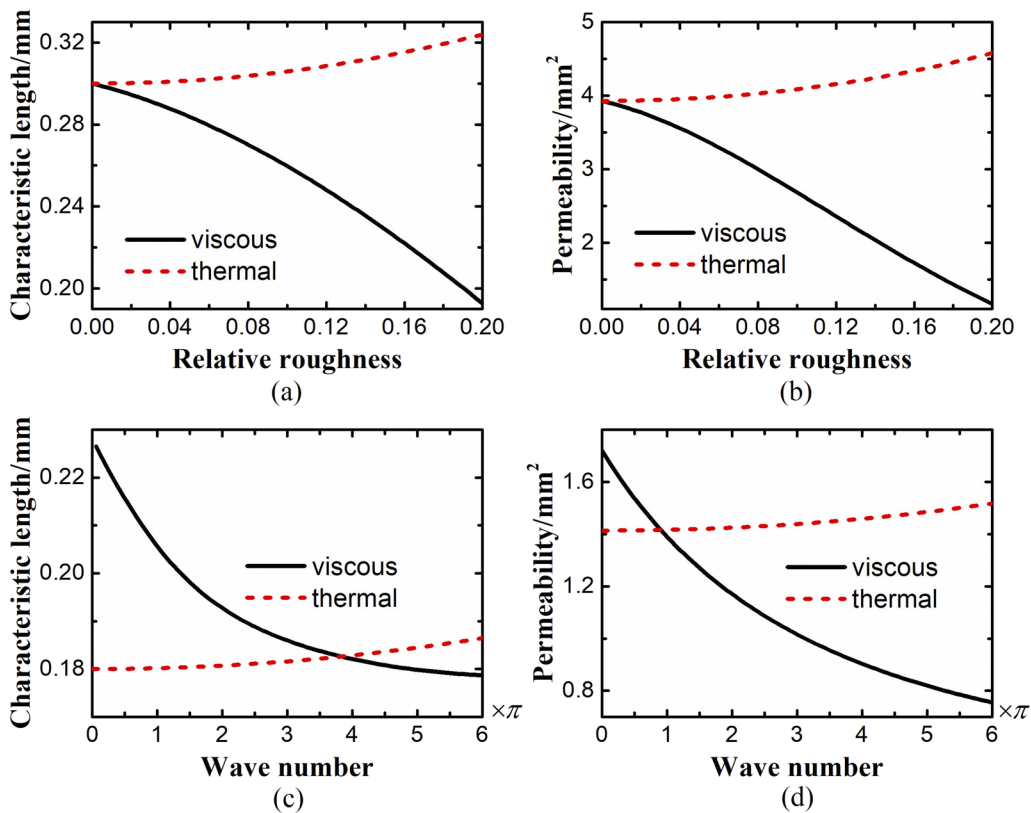


FIG. 6. Influence of roughness structure parameters on transport parameters: (a) influence of relative roughness on the characteristic length (at $\beta = 2\pi$), (b) influence of relative roughness on permeability (at $\beta = 2\pi$), (c) influence of wave number on the characteristic length (at $\varepsilon = 0.2$), and (d) influence of wave number on permeability (at $\varepsilon = 0.2$).

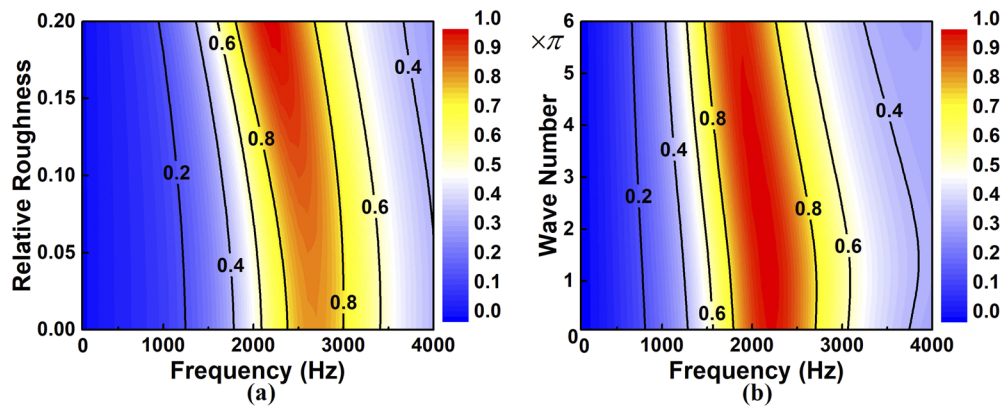


FIG. 7. Roughness effect on the sound absorption coefficient: (a) influence of relative roughness ϵ in contour map (at $\beta = 2\pi$) and (b) influence of wave number β in contour map (at $\epsilon = 0.2$).

therefore weakened by roughness, for a smaller temperature rise leads to a smaller energy loss. Different from the thermal effect, because of a larger flow resistivity [Eq. (5)], the sound wave suffers a larger viscous loss in rough tubes compared to the case of smooth tubes. Therefore, the viscous effect (i.e., viscous energy loss when a sound wave passes through a porous material) is strengthened by surface roughness.

For a rough tube in Fig. 2, the numerically calculated thermal permeability and viscous permeability are displayed in Fig. 4. In brief, thermal permeability relates to the difficulty of air to be compressed, while viscous permeability characterizes the difficulty of air to flow. When a sound wave travels across the rough tube, the air at positions with relatively small radii (i.e., the two ends of the tube in Fig. 4) is harder to be compressed compared to the air at positions with bigger radii (i.e., the middle of the tube in Fig. 4). Thus, there is a smaller thermal permeability at the two ends. As for the viscous permeability, because of a smaller section area, viscous permeability at the two ends is bigger than that at the middle, which is in agreement with the results of Fig. 4.

The sound absorption property of a porous material is strongly related with its surface impedance. By rewriting Eq. (15), the sound absorption coefficient can be expressed as $\alpha = \frac{4\text{Re}(z_n)}{[\text{Re}(z_n)+1]^2 + \text{Im}(z_n)^2}$, where $z_n = Z_s/Z_0$ is the normalized surface impedance. Figure 5 plots the real and imaginary parts of normalized surface impedance for both parallel rough tubes and smooth tubes. The equation of the sound absorption coefficient reveals that high sound absorption stems from appropriate acoustic resistance, i.e., $\text{Re}(Z_s/Z_0)$ close to 1, and low acoustic reactance, i.e., $\text{Im}(Z_s/Z_0)$ close to 0. As shown in Fig. 5, at the peak frequency (2290 Hz for rough tube and 2760 Hz for smooth tube; Fig. 3), one obtains $\text{Re}(Z_s/Z_0) = 0.75$ and $\text{Im}(Z_s/Z_0) = 0.10$ for the rough tube and $\text{Re}(Z_s/Z_0) = 0.45$ and $\text{Im}(Z_s/Z_0) = 0.08$ for the smooth tube, which validates the high sound absorption condition to certain extent.

Upon validating the sound absorption theory, the influence of roughness structure on transport parameters is quantified using the theory. As shown in Fig. 6, increasing either relative roughness or wave number leads to reduced viscous characteristic length and

viscous permeability but increased thermal characteristic length and thermal permeability. In fact, from Eqs. (4) and (8), the relationship between viscous permeability and viscous characteristic length can be derived as $\hat{k}_0 = \phi\Lambda^2/8\alpha_\infty$, implying that the viscous permeability is proportional to the square of the viscous characteristic length. From Eq. (12), the thermal permeability is found to be proportional to the square of thermal characteristic length. So, as shown in Fig. 6, the viscous characteristic length decreases with decreasing viscous permeability, while the thermal characteristic length increases with increasing viscous permeability.

Figure 7 plots the influence of relative roughness and wave number on the sound absorption coefficient. Figures 7(a) and 7(b) present the influence in the form of 2D contour maps, while Figs. 7(c) and 7(d) present the influence in a 3D manner. The sound absorption coefficient is depicted using different colors, ranging from blue to red as it increases in magnitude. As shown in Figs. 7(a)–7(d), with increasing relative roughness or wave number, the red region moves a little to the left and the area enlarges. That is, a larger relative roughness and a larger wave number can both decrease the resonant frequency and increase the sound absorption band of the porous material containing parallel rough tubes. As shown in Fig. 7(a), for the considered case, it is seen that if the relative roughness ϵ is less than 0.05, the roughness effect on the sound absorption can be negligible.

V. CONCLUSIONS

A theoretical model has been developed to characterize sound propagation in porous materials containing parallel rough tubes by taking into account the roughness effect on equivalent fluid properties in the Johnson–Champoux–Allard–Lafarge (JCAL) model. For simplicity, the rough tubes exhibit idealized sinusoidal morphologies. The predicted transport parameters (i.e., viscous permeability, thermal permeability, tortuosity, viscous characteristic length, and thermal characteristic length) and sound absorption coefficient are validated against finite element simulation results. Compared to a smooth tube, the rough tube achieves appropriate acoustic resistance and low acoustic reactance at a lower frequency, leading to a smaller

peak frequency and a higher peak sound absorption coefficient. Furthermore, the existence of surface roughness weakens the thermal effect and strengthens the viscous effect in sound energy dissipation. The present results are helpful for understanding the sound absorption behavior of porous materials containing rough tubes and enable designing high-performance sound absorbing materials by changing the surface roughness of micro-pores or micro-channels of porous materials.

AUTHORS' CONTRIBUTIONS

Z. Xu and W. He contributed equally to this manuscript.

ACKNOWLEDGMENTS

This work was supported by the NSFC (Grant Nos. 11761131003, U1737107, and 11772248), the DFG (Grant No. ZH15/32-1), and the Fundamental Research Funds for the Central Universities.

DATA AVAILABILITY

The data that support the findings of this study are available from the corresponding author upon reasonable request.

REFERENCES

- ¹G. Kirchhoff, "Ueber den einfluss der wärmeleitung in einem gase auf die schallbewegung," *Ann. Phys.* **210**, 177–193 (1868).
- ²J. W. S. Rayleigh, *The Theory of Sound* (Dover Publications, New York, 1945).
- ³F. D. Shields, K. P. Lee, and W. J. Wiley, "Numerical solution for sound velocity and absorption in cylindrical tubes," *J. Acoust. Soc. Am.* **37**, 724–729 (1965).
- ⁴H. A. Scarton and W. T. Rouleau, "Axisymmetric waves in compressible Newtonian liquids contained in rigid tubes: Steady-periodic mode shapes and dispersion by the method of eigenvallleys," *J. Fluid Mech.* **58**, 595–621 (1973).
- ⁵C. Zwikker and C. W. Kosten, *Sound Absorbing Materials* (Elsevier Publishing Company, Inc., New York, 1949).
- ⁶H. Tijdeman, "On the propagation of sound waves in cylindrical tubes," *J. Sound Vib.* **39**, 1–33 (1975).
- ⁷M. A. Biot, "Theory of propagation of elastic waves in a fluid-saturated porous solid. II. Higher frequency range," *J. Acoust. Soc. Am.* **28**, 179–191 (1956).
- ⁸K. Attenborough, "Acoustical characteristics of rigid fibrous absorbents and granular materials," *J. Acoust. Soc. Am.* **73**, 785–799 (1983).
- ⁹J. Allard and N. Atalla, *Propagation of Sound in Porous Media: Modelling Sound Absorbing Materials*, 2nd ed. (John Wiley & Sons, West Sussex, 2009).
- ¹⁰C. Colebrook and C. White, "Experiments with fluid friction in roughened pipes," *Proc. R. Soc. London, Ser. A* **161**, 367–381 (1937).
- ¹¹C. F. Colebrook, T. Blench, H. Chatley, E. H. Essex, J. R. Finnicome, G. Lacey, J. Williamson, and G. G. Macdonald, "Correspondence. Turbulent flow in pipes, with particular reference to the transition region between the smooth and rough pipe laws. (Includes plates)," *J. Inst. Civ. Eng.* **12**, 393–422 (1939).
- ¹²J. Nikuradse, "Laws of flow in rough pipes," NACA Technical Memorandum 1292, 1950.
- ¹³L. F. Moody, "Friction factors for pipe flow," *Trans. ASME* **66**, 671–684 (1944).
- ¹⁴C. Pozrikidis, "The flow of a liquid film along a periodic wall," *J. Fluid Mech.* **188**, 275–300 (1988).
- ¹⁵W. Qu, G. M. Mala, and D. Li, "Pressure-driven water flows in trapezoidal silicon microchannels," *Int. J. Heat Mass Transfer* **43**, 353–364 (2000).
- ¹⁶V. V. Dharaiya and S. G. Kandlikar, "A numerical study on the effects of 2d structured sinusoidal elements on fluid flow and heat transfer at microscale," *Int. J. Heat Mass Transfer* **57**, 190–201 (2013).
- ¹⁷I. Arenas, E. García, M. K. Fu, P. Orlandi, M. Hultmark, and S. Leonardi, "Comparison between super-hydrophobic, liquid infused and rough surfaces: A direct numerical simulation study," *J. Fluid Mech.* **869**, 500–525 (2019).
- ¹⁸S. Siddiqua, M. A. Hossain, and R. S. R. Gorla, "Natural convection flow of viscous fluid over triangular wavy horizontal surface," *Comput. Fluids* **106**, 130–134 (2015).
- ¹⁹X. Fang, Z. Yang, B.-C. Wang, M. F. Tachie, and D. J. Bergstrom, "Large-eddy simulation of turbulent flow and structures in a square duct roughened with perpendicular and V-shaped ribs," *Phys. Fluids* **29**, 065110 (2017).
- ²⁰J. Javaherchian and A. Moosavi, "Pressure drop reduction of power-law fluids in hydrophobic microgrooved channels," *Phys. Fluids* **31**, 073106 (2019).
- ²¹N. N. Anika, L. Djenidi, and S. Tardu, "Roughness effect in an initially laminar channel flow," *J. Fluid Mech.* **892**, A34 (2020).
- ²²S. Goswami and A. Hemmati, "Response of turbulent pipeflow to multiple square bar roughness elements at high Reynolds number," *Phys. Fluids* **32**, 075110 (2020).
- ²³Y. Lu, H. Liu, Z. Liu, and C. Yan, "Investigation and parameterization of transition shielding in roughness-disturbed boundary layer with direct numerical simulations," *Phys. Fluids* **32**, 074110 (2020).
- ²⁴S. Song, X. Yang, F. Xin, and T. J. Lu, "Modeling of surface roughness effects on Stokes flow in circular pipes," *Phys. Fluids* **30**, 023604 (2018).
- ²⁵S. Ren, F. Xin, T. J. Lu, and C. Zhang, "A semi-analytical model for the influence of temperature on sound propagation in sintered metal fiber materials," *Mater. Des.* **134**, 513–522 (2017).
- ²⁶X. Yang, S. Song, C. Yang, W. Hu, F. Han, L. Jin, and T. J. Lu, "Permeability model of micro-metal foam with surface micro-roughness," *Microfluid. Nanofluid.* **21**, 32 (2017).
- ²⁷R. Liu, L. Hou, W. Zhou, and Y. Chen, "Design, fabrication and sound absorption performance investigation of porous copper fiber sintered sheets with rough surface," *Appl. Acoust.* **170**, 107525 (2020).
- ²⁸R. Şimşek, "Vibration analysis of a single-walled carbon nanotube under action of a moving harmonic load based on nonlocal elasticity theory," *Physica E* **43**, 182–191 (2010).
- ²⁹D. L. Johnson, J. Koplik, and R. Dashen, "Theory of dynamic permeability and tortuosity in fluid-saturated porous media," *J. Fluid Mech.* **176**, 379–402 (1987).
- ³⁰Z. Xu, X. Peng, X. Liu, F. Xin, and T. J. Lu, "Modified theory of a microperforated panel with roughened perforations," *Europhys. Lett.* **125**, 34004 (2019).
- ³¹D. L. Johnson, J. Koplik, and L. M. Schwartz, "New pore-size parameter characterizing transport in porous media," *Phys. Rev. Lett.* **57**, 2564 (1986).
- ³²D. Lafarge, P. Lemarinier, J. F. Allard, and V. Tarnow, "Dynamic compressibility of air in porous structures at audible frequencies," *J. Acoust. Soc. Am.* **102**, 1995–2006 (1997).
- ³³Y. Champoux and J. F. Allard, "Dynamic tortuosity and bulk modulus in air-saturated porous media," *J. Appl. Phys.* **70**, 1975–1979 (1991).
- ³⁴S. Ren, Q. Ao, H. Meng, F. Xin, L. Huang, C. Zhang, and T. J. Lu, "A semi-analytical model for sound propagation in sintered fiber metals," *Composites, Part B* **126**, 17–26 (2017).
- ³⁵T. G. Zielinski, "Microstructure-based calculations and experimental results for sound absorbing porous layers of randomly packed rigid spherical beads," *J. Appl. Phys.* **116**, 034905 (2014).
- ³⁶M. Avellaneda and S. Torquato, "Rigorous link between fluid permeability, electrical conductivity, and relaxation times for transport in porous media," *Phys. Fluids A* **3**, 2529–2540 (1991).
- ³⁷D. Lafarge, "Comments on 'Rigorous link between fluid permeability, electrical conductivity, and relaxation times for transport in porous media'," *Phys. Fluids A* **5**, 500–502 (1993).
- ³⁸X. Wang and T. J. Lu, "Optimized acoustic properties of cellular solids," *J. Acoust. Soc. Am.* **106**, 756–765 (1999).